Acta Biomaterialia 6 (2010) 4506–4512

Contents lists available at ScienceDirect

Acta Biomaterialia

journal homepage: www.elsevier.com/locate/actabiomat

Ab initio study of thermodynamic, structural, and elastic properties of Mg-substituted crystalline calcite

Pavlína Elstnerová [a,b], Martin Friák [a,*], Helge Otto Fabritius [a], Liverios Lymperakis [a], Tilmann Hickel [a], Michal Petrov [a], Svetoslav Nikolov [c], Dierk Raabe [a], Andreas Ziegler [d], Sabine Hild [e], Jörg Neugebauer [a]

[a] Department of Computational Materials Design, Max-Planck-Institut für Eisenforschung GmbH, Max-Planck-Strasse 1, Düsseldorf 40237, Germany
[b] Department of Chemistry, Faculty of Science, Masaryk University, Kotlářská 2, Brno 611 37, Czech Republic
[c] Institute of Mechanics, Bulgarian Academy of Sciences, Acad. G. Bonchev Str. Bl. 4, 1113 Sofia, Bulgaria
[d] Central Facility for Electron Microscopy, University of Ulm, Albert-Einstein-Allee 11, Ulm 89069, Germany
[e] Department of Polymer Science, Johannes Kepler University Linz, Altenbergerstrasse 69, Linz 4040, Austria

ARTICLE INFO

Article history:
Received 21 April 2010
Received in revised form 9 July 2010
Accepted 14 July 2010
Available online 2 August 2010

Keywords:
Ab initio
Calcite
Stiffening
Mg-substitution
Elasticity

ABSTRACT

Arthropoda, which represent nearly 80% of all known animal species, are protected by an exoskeleton formed by their cuticle. The cuticle represents a hierarchically structured multifunctional biocomposite based on chitin and proteins. Some groups, such as Crustacea, reinforce the load-bearing parts of their cuticle with calcite. As the calcite sometimes contains Mg it was speculated that Mg may have a stiffening impact on the mechanical properties of the cuticle (Becker et al., Dalton Trans. (2005) 1814). Motivated by these facts, we present a theoretical parameter-free quantum-mechanical study of the phase stability and structural and elastic properties of Mg-substituted calcite crystals. The Mg-substitutions were chosen as examples of states that occur in complex chemical environments typical for biological systems in which calcite crystals contain impurities, the role of which is still the topic of debate. Density functional theory calculations of bulk $(Ca,Mg)CO_3$ were performed employing 30-atom supercells within the generalized gradient approximation as implemented in the Vienna Ab-initio Simulation Package. Based on the calculated thermodynamic results, low concentrations of Mg atoms are predicted to be stable in calcite crystals in agreement with experimental findings. Examining the structural characteristics, Mg additions nearly linearly reduce the volume of substituted crystals. The predicted elastic bulk modulus results reveal that the Mg substitution nearly linearly stiffens the calcite crystals. Due to the quite large size-mismatch of Mg and Ca atoms, Mg substitution results in local distortions such as off-planar tilting of the CO_3^{2-} group.

In the course of evolution nature has developed numerous materials with outstanding functional and structural properties. These structures mostly consist of an organic matrix of structural biopolymers which is modified and reinforced with various proteins and biominerals [1–9]. Such materials possess excellent stiffness, toughness, and strength related to their low density, while the mechanical characteristics of their underlying constituents are rather modest [8,10]. This remarkable performance is a consequence of their hierarchical structure, the specific design at each level of organization and the inherent strong heterogeneity [10]. Therefore, to understand macroscopic mechanical properties of these materials, one should take into account their structure–property relations at all length scales down to the molecular level. Hence, multiscale modeling that can systematically describe and investigate material properties from the atomistic scale up to the macroscopic level has become the most widely used method for tackling the structure–property relations of biological nanocomposites and has been applied to bone, nacre, mother of pearl, arthropod cuticle, and other materials (e.g. [7,11–16]).

Recently Nikolov et al. [17,16] developed a bottom-up multiscale approach to model hierarchically structured nanocomposites. This approach combines quantum mechanical *ab initio* calculations with hierarchical homogenization continuum methods and has been successfully applied to study the elastic properties of the chitin-based mineralized cuticle of an arthropod, the lobster *Homarus americanus*. In this hierarchical constitutive model *ab initio* calculations are used to describe the ground-state structure and elastic properties of chitin which are relevant on the nanometer-scale where experimental data are missing. However, the properties of these materials do not depend only on the specific microstructure at all levels of hierarchy but also on the chemical composition of both the organic and inorganic components. Among the over 60 different biogenic minerals known at

* Corresponding author. Tel.: +49 211 67 92 461.
E-mail address: friak@mpie.de (M. Friák).

1742-7061/$ - see front matter © 2010 Acta Materialia Inc. Published by Elsevier Ltd. All rights reserved.
doi:10.1016/j.actbio.2010.07.015

present [1–4,6], Ca carbonate is the most widespread biomineral used by invertebrates. It serves as the skeletal element in the shells of marine protists and corals, as material for the shells of molluscs and echinoderms, and in the exoskeletons of crustaceans [18]. In these organisms, it occurs either in its amorphous form (ACC) or as crystalline calcite, which is frequently associated with significant amounts of Mg. In crustaceans, the presence of Mg calcite has been shown for a number of species [19,20], and an Mg content as high as 11% was reported in biogenic calcite samples taken from the spines and the body skeleton of the sea urchin *Paracentrotus lividus* [21]. It was speculated [22] that the Mg content may affect the mechanical properties of the cuticle since Mg calcite is harder than calcite without Mg, suggesting that it is formed for mechanical reasons. Fig. 1a shows an electron micrograph of a microtome polished cross-section from the dorsal carapace of a large decapod crustacean, the edible crab *Cancer pagurus* and its elemental composition measured by energy dispersive X-ray spectrometry (EDX), showing the presence of Ca, O, C, P, Ca and Mg. Qualitative EDX mappings show the heterogeneous distribution of Ca (Fig. 1b), Mg (Fig. 1c) and P (Fig. 1d) in the two mechanically relevant main layers, the exocuticle and endocuticle. Similar inhomogeneous distributions of organic and inorganic components within crustacean cuticles have been reported earlier [23,24], and were correlated to the functions of particular skeletal elements. Ca carbonate plays a generally important role in the structure and mechanic properties of these materials. However, there is still an ongoing debate about the specific role of Mg. In addition to enhancing the mechanical properties of calcite, it has also been proposed that Mg^{2+} ions can block the formation of calcite in the presence of biopolymers and therefore favour precipitation of amorphous $CaCO_3$ [25]. Studying the thermodynamic, structural, and elastic properties of Mg-substituted crystalline calcite on the molecular level can help to gain a deeper understanding of the role Mg plays in biological materials.

Previous theoretical calculations, based on valence force field as well as *ab initio* methods, on the system of Ca and Mg carbonates have focused on the thermodynamics, structural, vibrational and elastic properties for the stoichiometric end-members of the pseudobinary alloy system $Ca_nMg_m(CO_3)_{n+m}$ [26–35]). The energetics and atomic geometry of Mg-substitutions in calcite have been addressed by using Hartree–Fock linear-combination-of-atomic-orbitals (HF-LCAO) calculations [36]. However, a detailed study on the atomic geometry, the energetics, and the elastic properties of the pseudobinary alloy system $Ca_nMg_m(CO_3)_{n+m}$ for the whole range of compositions is lacking. Therefore, in the present study we focus on the mineral matrix inhomogeneities and address the elastic properties of calcite ($CaCO_3$), magnesite ($MgCO_3$) and the pseudobinary alloy system $Ca_nMg_m(CO_3)_{n+m}$.

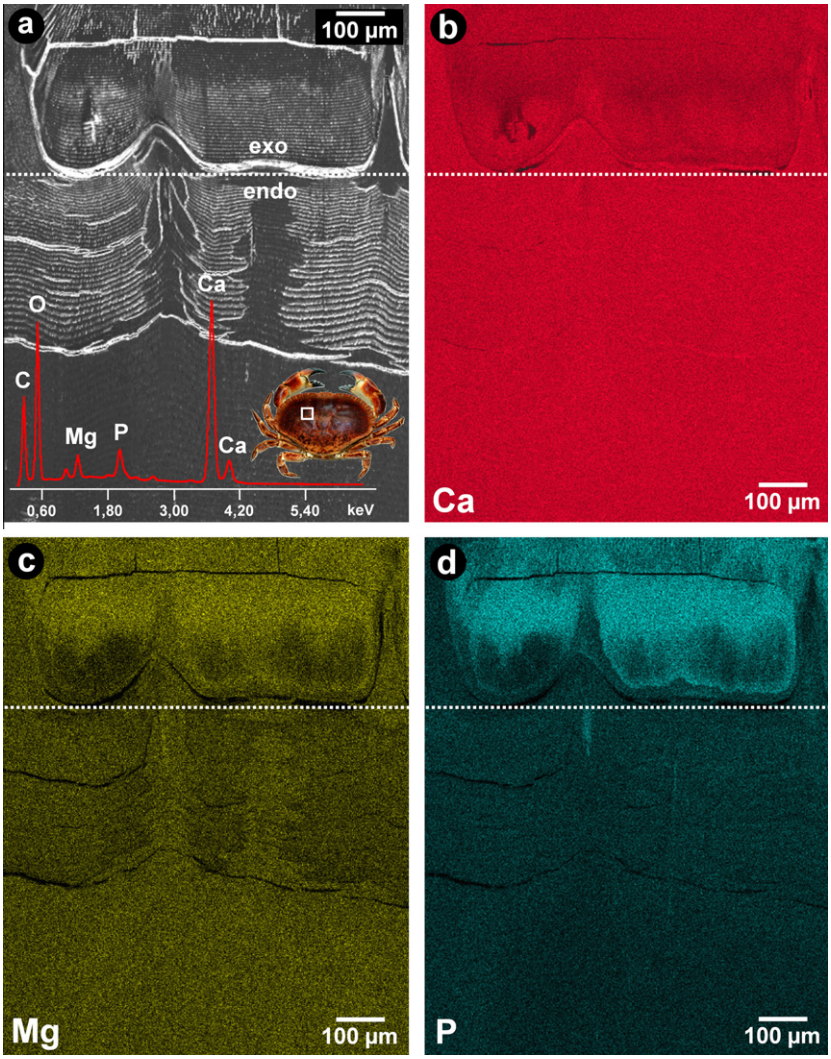

Fig. 1. Elemental distribution in cuticle from the dorsal carapace of the crab *Cancer pagurus*. (a) Electron micrograph of a microtome-polished cross-section showing the two structurally different main layers exocuticle (exo) and endocuticle (endo) and the elemental composition measured by qualitative energy dispersive X-ray spectrometry (EDX). (b–d) Qualitative EDX mapping showing the heterogeneous distribution of Ca (b), Mg (c) and P (d) throughout the thickness of the cuticle.

1. Methodology

$CaCO_3$ is a common carbon-bearing mineral found on the Earth's surface and mantle [37]. $CaCO_3$ and $MgCO_3$ crystallize under ambient conditions in the hexagonal/rhombohedral $R\bar{3}c$ phase layered structure in which CO_3^{2-} planes alternate with cation (Ca^{2+} or Mg^{2+}) ones (see Fig. 2). The rhombohedral unit cell of these carbonates contains two formula units and thus 10 atoms. The reduced coordinates of the cation atoms are (0,0,0) and $(\frac{1}{2},\frac{1}{2},\frac{1}{2})$, of the C atoms $(\frac{1}{4},\frac{1}{4},\frac{1}{4})$ and $(\frac{3}{4},\frac{3}{4},\frac{3}{4})$, and of the O atoms $(u,\frac{1}{2}-u,\frac{1}{4})$, $(\frac{1}{4},u,\frac{1}{2}-u)$, $(\frac{1}{2}-u,\frac{1}{4},u)$, $(u,\frac{1}{2},+u,\frac{3}{4})$, $(\frac{3}{4},u,\frac{1}{2}+u)$, and $(\frac{1}{2}+u,\frac{3}{4},u)$, in units of the primitive vectors $(a,0,c)$, $\left(-\frac{1}{2}a,\frac{\sqrt{3}}{2}a,c\right)$, and $\left(-\frac{1}{2}a,-\frac{\sqrt{3}}{2}a,c\right)$, where u is the internal lattice parameter and a and c are the lattice constants. The hexagonal elementary cell is three times bigger and it contains 6 formula units and 30 atoms. Since most of the previous studies [26–30,32–35] published the structural parameters (e.g. the equilibrium volume) with respect to the 30-atom elementary cell (rather then to the formula unit) we keep this nomenclature throughout this work. Since a single supercell contains 6 formula units of calcite, 6 different ratios of Ca and Mg atoms could be studied.

Our calculations are based on density functional theory (DFT) [38,39] using the generalized gradient approximation (GGA) [40] and the projected augmented wave approach (PAW) as implemented in the Vienna Ab-initio Simulation Package (VASP) code [41–43]. The GGA was chosen due to its satisfactory performance in the studied class of materials (e.g. [44–47]). The plane-wave cut-off energy was 390 Ry and a $4\times 8\times 6$ Monkhorst–Pack mesh was used to sample the Brillouin zone of the 30-atom supercells (see Fig. 3). Convergence with respect to cutoff energy and k-point sampling has been explicitly checked.

2. Results for calcite and magnesite

The equilibrium structural and elastic characteristics are summarized in Table 1 for calcite and in Table 2 for magnesite together with previously calculated values and experimental data. As seen in Tables 1 and 2, our results are in close agreement with the experimental data. The equilibrium volumes are slightly overestimated for both carbonates and the bulk moduli are slightly underestimated as compared to experimental data but the qualitative trends are well reproduced. The calculated larger equilibrium volume is attributed to the use of GGA for the exchange and correlation potential, which is well known to slightly overestimate the lattice constant and slightly underestimate the bulk modulus (e.g. [44–46]).

As far as the interatomic distances are concerned, it is interesting to note that the distances within the CO_3^{2-} groups are nearly independent of the composition of the actual carbonate. The C–O distance differs only by 0.23% in $CaCO_3$ and $MgCO_3$, being a bit smaller in the latter. This is in agreement with both previous theoretical studies and experimental findings as listed in Tables 1 and 2. In contrast, the Ca–O or Mg–O interatomic distances are predicted to differ substantially (10.82%) in the two studied compounds in agreement with previous theoretical and experimental findings. This can be explained in terms of the larger atomic radius of a Ca atom with respect to a Mg atom. This is clearly depicted in Table 3: the volume per atom in the face-centered cubic (fcc) Ca ground state is almost two times larger than the corresponding volume in the experimentally observed ambient-condition ground state hexagonal close-packed (hcp) Mg. Furthermore, the experimental nearest neighbor distance, 3.95 Å in fcc Ca [52], is larger than the corresponding distance, 3.20 Å, in hcp Mg [53].

In order to examine how pressure affects the structure, we plot in Fig. 4 the dependence of the interatomic bonds as function of the applied hydrostatic strain. In agreement with a previous theoretical study by Catti et al. [27], three different trends for the interatomic distance can be seen. The interlayer Ca–O and Mg–O distances (see Fig. 2) show the strongest response upon volumetric changes. The response of the interplanar Ca–Ca and Mg–Mg lengths are less sensitive and the smallest changes are in the length of C–O bonds within the CO_3^{2-} groups. These differences in the behavior of the C–O bonds with respect to the other bonds indicate the different character (covalent vs. ionic) and strength of interatomic bonding in the studied compounds. A similar behavior has been observed for transition-metal (TM) disilicides in response to tensile loading [57,58]) where Si–Si and TM–Si bonds with dif-

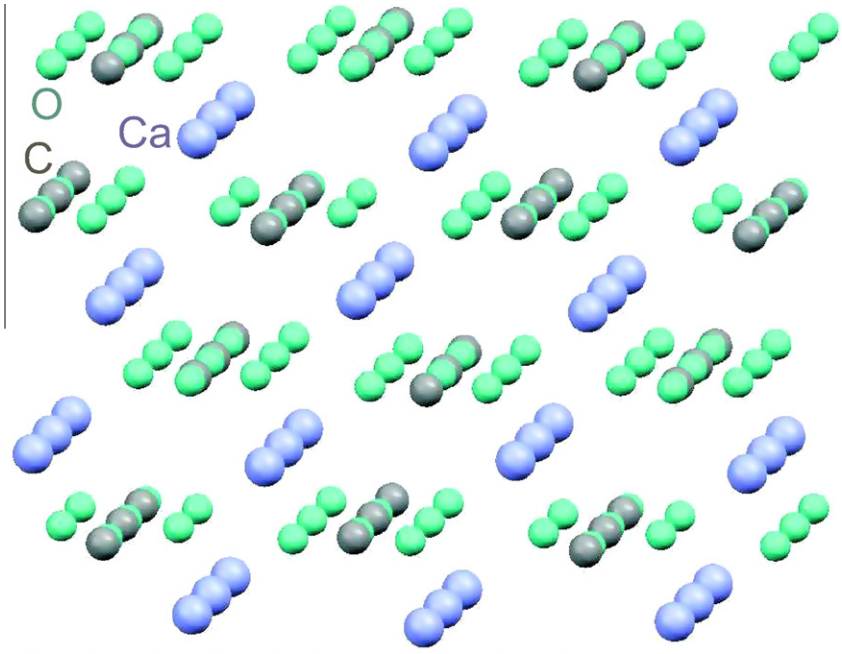

Fig. 2. Layered crystalline structure of $CaCO_3$. The Ca atoms are visualized as light-blue sphere, O atoms as light-green spheres, and C as gray spheres.

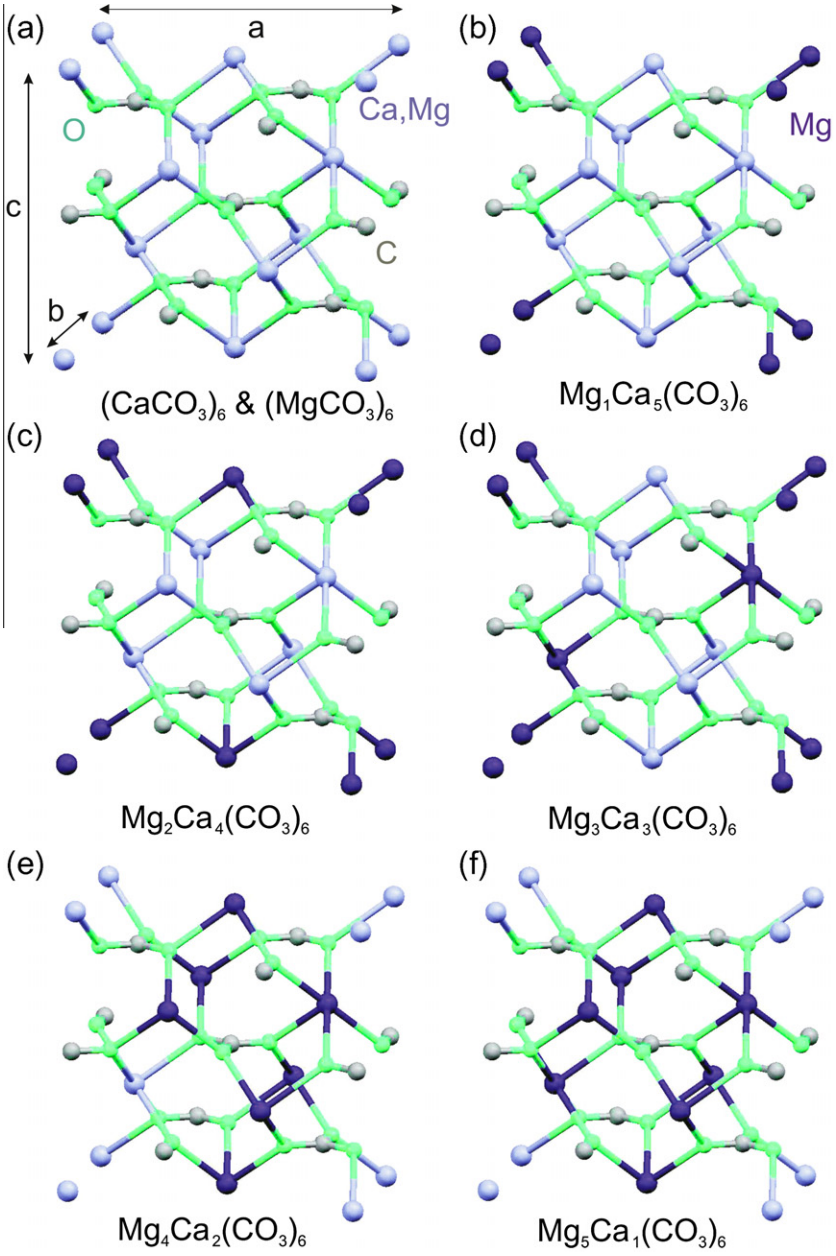

Fig. 3. Schematic visualization of the 30-atom supercells used to model compounds with different Mg:Ca atomic ratios. The Ca atoms are visualized as light-blue spheres, Mg atoms as dark-blue spheres, O atoms as light-green spheres, and C as gray spheres. The supercell lattice parameters a, b, c are defined in (a).

Table 1
Theoretically predicted structural and elastic parameters of $CaCO_3$ in comparison with values obtained in previous theoretical studies and experiments. Specifically, the equilibrium volume V (Å) of the 30-atom (6 formula units) supercells is listed together with the corresponding bulk modulus B_0, its pressure derivative B_0' and C–O and Ca–O interatomic distances (Å).

$CaCO_3$	V/6 f.u. (Å^3)	B_0 (GPa)	B_0'	C–O (Å)	Ca–O (Å)
This work	383.7	69.6	4.54	1.300	2.396
Previous calculations	364-386	73-75	4.63	1.270	2.415
	[26,27]	[26,27]	[27]	[27]	[27]
Exp.	367.8	80	–	1.283	2.354
	[48,49]	[48]	–	[50]	[50]

Table 2
As in Table 1 but for $MgCO_3$.

$MgCO_3$	V/6 f.u. (Å^3)	B_0 (GPa)	B_0'	C–O (Å)	Mg–O (Å)
This work	293.4	96	4.97	1.297	2.15
Previous calculations	279.2	124	3.08	1.286	2.11
	[28]	[28]	[28]	[28]	[27]
Exp.	278.5	117	–	1.287	2.10
	[48]	[51]	–	[50]	[50]

ferent strengths can be identified. Moreover, the stability of the CO_3^{2-} group is probably related to the fact that the frequency of the A_{1g} Raman active phonon mode associated with this group was experimentally found to be nearly equal in a broad class of carbonates [59], including not only $CaCO_3$ and $MgCO_3$ but also $CdCO_3$, $FeCO_3$, $NiCO_3$, $ZnCO_3$ and $MnCO_3$. The frequencies detected in these seven carbonates cover a very narrow range with the maximum of 1090 cm^{-1} measured in $ZnCO_3$ and the minimum frequency of 1084 cm^{-1} detected in $CdCO_3$.

Table 3
Theoretically predicted equilibrium lattice parameters (in Å) and corresponding bulk moduli B (GPa) of fcc Ca and hcp Mg in comparison with (i) values obtained in previous theoretical studies [54,55] employing both the VASP code and the all-electron full-potential WIEN2k package and (ii) experimental data [52,56,53]. Small differences in, for example, equilibrium volume between our theoretical predictions and previous VASP results can be assigned to different computational parameters used in the previous study, which focused on Mg–Li solid solutions, and in which different values of the parameters were needed due to the presence of Li.

	This study	VASP	WIEN2k	Exp.
a_{fcc}^{Ca} (Å)	5.53	5.49 [54]	5.55 [54]	5.59 [52]
B_{fcc}^{Ca} (GPa)	17.3	–	–	17.0
V_{fcc}^{Ca} (Å^3/atom)	42.3	41.4 [54]	42.7 [54]	43.7 [52]
a_{hcp}^{Mg}(Å)	3.20	3.18 [54]	3.19 [54]	3.21 [53]
c_{hcp}^{Mg} (Å)	5.18	5.17 [54]	5.18 [54]	5.21 [53]
B_{hcp}^{Mg} (GPa)	35.5	34.8 [55]	–	35.4 [56]
V_{hcp}^{Mg} (Å^3/atom)	22.98	23.03 [55]	22.85 [54]	23.25 [53]

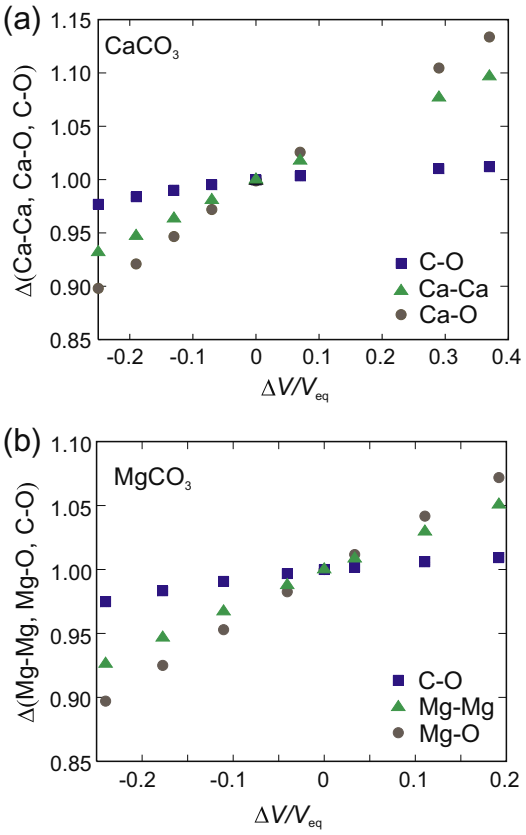

Fig. 4. Relative changes (Δ) of the interatomic bonds are shown as a function of volume for calcite (a) and magnesite (b). The equilibrium length is set to be equal to 1 in both cases.

3. Results for substituted states

In the previous section the properties of Ca and Mg carbonates have been addressed. Here we focus on the pseudobinary $Ca_nMg_m(CO_3)_{n+m}$ alloy system where Ca and Mg atoms occupy the cation sublattice sites. Other substitutional or interstitial positions were not assumed in the present study. The cation sublattice sites are energetically preferred over the other sites and this type of substitution thus coheres with the well-known chemical preferences of the present elements with respect to, for example, preferred coordination number or ionization state. The five types of pseudobinary supercells are shown in Fig. 3b–f. We note that they do not cover the whole configurational space of the 30-atom structures. Nevertheless, this choice constitutes a representative set of structures and provides an efficient approach to investigate and identify the dependence of the energetics, atomic geometry and elastic properties on the alloy composition.

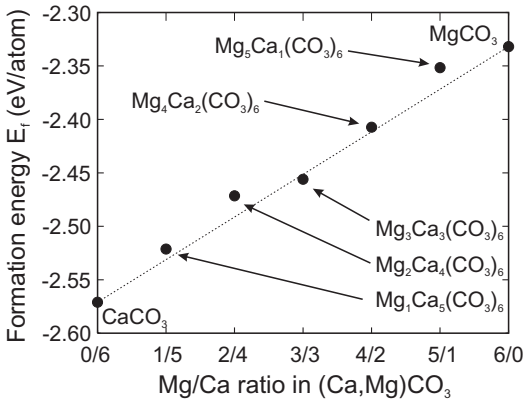

Fig. 5. The compositional dependence of the formation energy E_f (eV/atom) calculated for the supercells shown in Fig. 3.

The formation energy E_f of a Ca_n $Mg_m(CO_3)_{n+m}$ alloy consisting in total of $5(n+m) = N$ atoms can be written as follows:

$$E_f = \frac{E^{tot} - n\mu^{Ca} - m\mu^{Mg} - (n+m)\mu^{C} - 3(n+m)\frac{1}{2}\mu^{O_2}}{N},$$

where E^{tot} is the total energy of the Ca_n $Mg_m(CO_3)_{n+m}$ system and the chemical potentials μ are energies per atoms of the constituents in their ambient-condition ground-state phases. The fcc, hcp, graphite phase and a 2-atom molecule have been assumed as the ground state phases for the Ca, Mg, C and O, respectively. The formation energy as function of the composition (n_{Ca}/m_{Mg}) is shown in Fig. 5. The formation energies of the computed compounds nearly follow a linear rule of mixture indicated by the tie-line connecting both carbonate end-members. Moreover, all the energies are above this line except for the formation energy of the compound with an equal number of Mg and Ca atoms. The energy of this structure is slightly below the tie-line, indicating a thermodynamically stable compound. However, the experimentally detected ground state phase in this concentration region is dolomite, i.e. a trigonally distorted crystal structure with a lower symmetry (space group $R\bar{3}$). In fact, the energy gain of 15 meV/atom of this structure compared to the tie-line is rather small.

The compositional dependence of the equilibrium volume V (Å^3/6 f.u.) and the bulk moduli B (GPa) are shown in Table 4 and in Fig. 6. The equilibrium volume is found to decrease monotonically with increasing Mg content (Fig. 6a). This finding reflects the fact that bigger Ca atoms are being replaced by smaller Mg atoms.

Table 4
Theoretically predicted equilibrium volumes (in Å^3 per 6 formula units), bulk moduli B (GPa) and formation energies E_f (in eV/atom) of the computed substituted states.

	V_{eq} (Å^3/6 f.u.)	B (GPa)	E_f (eV/atom)
$CaCO_3$	383.36	70.3	−2.571
$Mg_1Ca_5(CO_3)_6$	365.2	74.1	−2.521
$Mg_2Ca_4(CO_3)_6$	350.8	82	−2.472
$Mg_3Ca_3(CO_3)_6$	332.9	85.7	−2.456
$Mg_4Ca_2(CO_3)_6$	318.0	89.4	−2.407
$Mg_5Ca_1(CO_3)_6$	307.0	93.9	−2.352
$MgCO_3$	293.92	100.1	−2.310

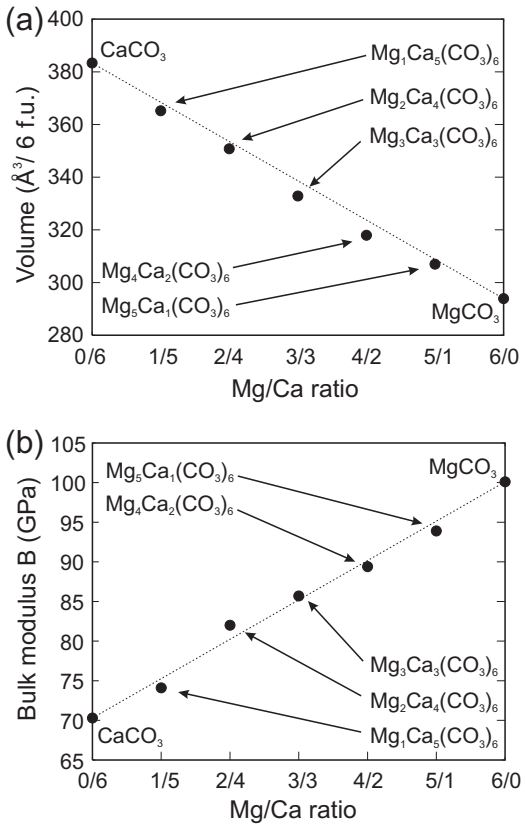

Fig. 6. The compositional dependence of (a) the equilibrium volume V (Å^3/6 f.u.) and (b) corresponding bulk moduli B (GPa) calculated for the supercells shown in Fig. 3.

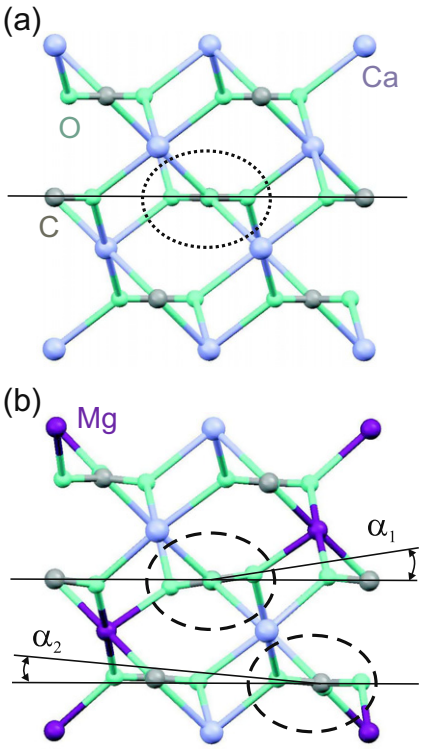

Fig. 7. Side-view (b–c plane; see Fig. 3a) of the 30-atom supercells of (a) stoichiometric calcite with in-plane oriented CO_3^{2-} groups (see the dotted oval) and (b) locally tilted CO_3^{2-} groups (see the dashed oval) in the equilibrium state of substituted $Mg_3Ca_3(CO_3)_6$. The off-planar tilt angles α_1 and α_2 in (b) have values of ≈7° and ≈5°, respectively.

Moreover, the deviation of the volume from Vegard's law is rather small: assuming an extended Vegard's law with a bowing parameter b ($V_{Mg_xCa_{1-x}CO_3} = xV_{MgCO_3} + (1-x)V_{CaCO_3} - bx(1-x)$), the bowing parameter is found to be $b = 22.96$ Å^3. As the volume decreases with increasing Mg content, interactions between the atoms become exceedingly stiff due to Pauli repulsion. This effect is related to the well-known asymmetry in the chemical bond: decreasing the bond distance (i.e. reducing the volume) gives rise to a strong repulsive interaction due to core–core interaction, while increasing the bond length results in a much weaker attractive interaction due to weakening of the electronic bond. As a consequence the mechanical response (second derivative of the bond energy with respect to bond length) is highly asymmetric and becomes larger (smaller) when decreasing (increasing) the bond length. This explains why the bulk modulus is found to increase with decreasing volume (see Fig. 6b). The increase is almost linear with a slope of 0.3 GPa/at.% Mg. Therefore, increasing the Mg content in the Mg–Ca pseudobinary alloy, the system will in turn increase the overall stiffness of the calcite crystals. Similar linear compositional trends of the bulk modulus were predicted also in other systems (e.g. [60]). An Mg content close to that of dolomite, specifically 45 mol.% recently reported by Ma et al. [61], is predicted to result in an increase in the bulk modulus from 70.3 GPa (in the stoichiometric calcite) to 83.8 GPa.

Substituting Ca atoms by Mg atoms (which are nearly half the size) in the calcite crystal will not only affect the overall stiffness of the crystal but will also result in rather high internal lattice strains and stresses. Consequently, the lattices exhibit significant structural distortions. This is clearly demonstrated in Fig. 7a and b:by substituting half of the Ca atoms by Mg atoms a strong tilt ≈6° of the CO_3^{2-} groups from their planar configuration is observed. The structural distortions induced by the internal strains are further highlighted in Fig. 8. The cation–C as well as the Mg–Ca interatomic distances can vary as much as ≈14% over the whole compositional range. In contrast, the C–O within the CO_3^{2-} as well as the cation–O interatomic distances are not affected and remain practically constant. The aforementioned internal strains are very likely to prevent the formation of crystals with Mg concentrations close to 50 at.% under equilibrium conditions. The fact that crystalline structures with substantial Mg substitutions are experimentally found (e.g. [21]) is thus a clear indication of non-equilibrium conditions as frequently encountered in biological systems. The Mg concentrations measured in crustacean cuticles are in the range of 0.5–2 wt.% [19,20] for the bulk material, but locally higher concentrations cannot be ruled out due to the inhomogeneous distribution of minerals in these materials. Indeed, a recent study of the grinding tip of a sea urchin tooth has reported Mg concentrations of the polycrystalline matrix close to that of dolomite, namely ≈45 mol.% [61].

4. Conclusions

We have investigated energetics, atomic geometry and elastic properties of $CaCO_3$ and $MgCO_3$ carbonates as well as of the corresponding $Ca_nMg_m(CO_3)_{n+m}$ pseudobinary alloys, by employing *ab initio* calculations. Our predictions indicate that low concentrations of Mg atoms do not lead to a destabilization of calcite crystals. The dependence of the equilibrium volume on the alloy composition is found to exhibit a rather small bowing parameter. In contrast to the volume, the bulk modulus is found to increase with increasing Mg content at a slope of 0.3 GPa/at.% Mg. This finding can be understood in terms of the different Ca and Mg atomic volumes: the Ca atom is almost twice as large as the Mg atom.

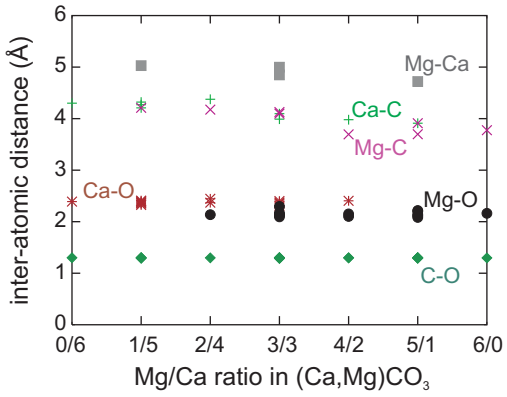

Fig. 8. Dependence of the cation–C, cation–O, Mg–Ca, and C–O interatomic distances on the composition.

Substituting Ca by Mg decreases the volume of the alloy. Moreover, the interatomic interactions are exerted over small distances, resulting in a stiffer material. Additionally, the different atomic volumes of the two cations result in large internal strains in the pseudobinary alloys. These internal stresses result in local distortions such as off-planar tilting of the CO_3^{2-} groups. The effect of the stresses on the atomic geometry depends strongly on the nature of the corresponding interatomic bonds. For example, the C–O bonds within the CO_3^{2-} group are nearly unaffected by the internal stresses and show only a very weak dependence on externally applied stresses. In contrast, our results clearly show that cation–cation interatomic distances are more sensitive to both internal and external applied stress. Considering the bulk modulus increase with increasing Mg content, the *ab initio* results thus support earlier speculations [22] that one of the reasons why Mg additions occur in calcite-containing biocomposites is their stiffening impact on the mechanical properties that unfortunately occurs at expense of structural and thermodynamic stability. Even more importantly, these calculations provide direct insight into the principles underlying this biologically important hardening mechanism.

Acknowledgments

This research was supported (i) by the Deutsche Forschungsgemeinschaft (DFG) (project "Crustacean skeletal elements: variations in the constructional morphology at different hierarchical levels") within the priority program (SPP) 1420 "Biomimetic materials research: functionality by hierarchical structuring of materials", (ii) by the Grant Agency of the Czech Republic (projects Nos. 202/09/1786 and 106/09/H035) and (iii) by the Research Project MSM0021622410. M.F. would like to acknowledge funding by the Interdisciplinary Centre for Materials Simulation (ICAMS), which is supported by ThyssenKrupp AG, Bayer MaterialScience AG, Salzgitter Mannesmann Forschung GmbH, Robert Bosch GmbH, Benteler Stahl/Rohr GmbH, Bayer Technology Services GmbH and the state of North-Rhine Westphalia as well as the European Commission in the framework of the European Regional Development Fund (ERDF).

Appendix A. Figures with essential colour discrimination

Certain figures in this article, particularly Figures 1–4, 7 and 8, are difficult to interpret in black and white. The full colour images can be found in the on-line version, at doi:10.1016/j.actbio.2010.07.015).

References

[1] Lowenstam HA. Science 1981;211:1126.
[2] Mann S, Webb J, Williams RJP. On biomineralization. New York: VCH Press; 1989.
[3] Lowenstam HA, Weiner S. On biomineralization. New York: Oxford University Press; 1989.
[4] Mann S. J Mater Chem 1995;5:935.
[5] Manoli F, Koutsopoulos S, Dalas E. J Cryst Growth 1997;182:116.
[6] Weiner S, Addadi L. J Mater Chem 1997;7:689.
[7] Fratzl P, Weinkamer R. Prog Mater Sci 2007;52:1263.
[8] Meyers MA, Chen PY, Lin AYM, Seki Y. Prog Mater Sci 2008;53:1.
[9] Buehler MJ, Keten S, Ackbarow T. Prog Mater Sci 2008;53:1101.
[10] Tai K, Dao M, Suresh S, Palazoglu A, Ortiz C. Nat Mater 2007;6:454.
[11] Vincent JFV, Wegst UGK. Arthropod Struct Dev 2004;33:187.
[12] Ashby MF, Wegst UGK. Phil Mag 2004;84:2167.
[13] Raabe D, Romano P, Sachs C, Fabritius HO, Al-Sawalmih A, Yi S-B, et al. Mater Sci Eng A 2006;421:143.
[14] Nikolov S, Raabe D. Biophys J 2008;94:4220.
[15] Fabritius H, Sachs C, Romano P, Raabe D. Adv Mater 2009;21:391.
[16] Nikolov S, Petrov M, Lymperakis L, Friák M, Fabritius HO, Raabe D, et al. Adv Mater 2010;22:519.
[17] Nikolov S, Sachs C, Fabritius H, Raabe D, Petrov M, Friák M, et al. In: El-Azab A, editor. Proceedings of the fourth international conference on multiscale materials modeling (MMM-2008), tackling materials complexities via computational science. Department of Scientific Computing, Florida State University, Tallahassee, FLA, USA; 2008. p. 667–670.
[18] Meldrum FC. Int Mater Rev 2003;48:187.
[19] Neues F, Ziegler A, Epple M. Cryst Eng Commun 2007;9:1245.
[20] Boßelmann F, Romano P, Fabritius H, Raabe D, Epple M. Thermochim Acta 2007;463:65.
[21] Zolotoyabko E, Caspi EN, Fieramosca JS, Dreele RBV, Marin F, Mor G, et al. Cryst Growth Des 2010;10:1207.
[22] Becker A, Ziegler A, Epple M. Dalton Trans 2005:1814.
[23] Hild S, Marti O, Ziegler A. J Struct Bio 2008;163:100.
[24] Hild S, Neues F, Žnidaršič N, Štrus J, Epple M, Marti O, et al. J Struct Biol 2009;168:426.
[25] Raz S, Weiner S, Addadi L. Adv Mater 2000;12:38.
[26] Pavese A, Catti M, Price GD, Jackson RA. Phys Chem Miner 1992;19:80.
[27] Catti M, Pavese A, Aprà E, Roetti C. Phys Chem Miner 1993;20:104.
[28] Catti M, Pavese A, Dovesi D, Saunders VR. Phys Rev B 1993;47:9189.
[29] Catti M, Pavese A, Price GD. Phys Chem Miner 1993;19:472.
[30] Pavese A, Catti M, Parker SC, Wall A. Phys Chem Miner 1996;23:89.
[31] Burton BP, Van de Walle A. Phys Chem Miner 2003;30:88.
[32] Prencipe M, Pascale F, Zicovich-Wilson CM, Saunders VR, Orlando R, Dovesi R. Phys Chem Miner 2004;31:559.
[33] Valenzano L, Noël Y, Orlando R, Zicovich-Wilson CM, Ferrero M, Dovesi R. Theor Chem Acc 2007;117:991.
[34] Akbarzadeh H, Shokouhi M, Parsafar GA. Mol Phys 2008;106:2545.
[35] Kawano J, Miyake A, Shimobayashi N, Kitamura M. J Phys: Condens Matter 2009;21:095406.
[36] Menadakis M, Maroulis G, Koutsoukos PG. Computat Mater Sci 2007;38:522.
[37] Ono S, Kikegawa T, Ohishi Y. Am Miner 2007;92:1246.
[38] Hohenberg P, Kohn W. Phys Rev 1964;136:B864.
[39] Kohn W, Sham LJ. Phys Rev 1965;140:A1133.
[40] Perdew JP, Burke K, Ernzerhof M. Phys Rev Lett 1996;77:3865.
[41] Kresse G, Hafner J. Phys Rev B 1993;47:558.
[42] Kresse G, Furthmüller J. Phys Rev B 1996;54:11169.
[43] Blöchl PE. Phys Rev B 1994;50:17953.
[44] Zupan A, Causa M. Int J Quant Chem 1995;56:337.
[45] Moroni EG, Kresse G, Hafner J, Furthmüller J. Phys Rev B 1997;56:15629.
[46] Zoroddu A, Bernardini F, Ruggerone P, Fiorentini V. Phys Rev B 2001;64:045208.
[47] Ireta J, Neugebauer J, Scheffler M. J Phys Chem A 2004;108:5692.
[48] Effenberger H, Mereiter K, Zemann J. Z Kristallogr 1981;156:233.
[49] Leeuw NHD. J Phys Chem B 2002;106:5241.
[50] Markgraf SA, Reede RJ. Am Minerl 1985;70:590.
[51] Pandekar DP, Ruoff AL. J Appl Phys 1968;39:6004.
[52] King HW. Bull Alloy Phase Diagr 1981;2:401.
[53] Kittel C. In: Introduction to solid state physics. New York: Wiley; 1976. p. 31, 75, 85.
[54] Zhong Y, Ozturk K, Sofo JO, Liu Z-K. J Alloys Compd 2006;420:98.
[55] Counts WA, Friák M, Raabe D, Neugebauer J. In: Kainer KU, editor. Magnesium, 8th international conference on magnesium alloys and their applications. Weinheim: Wiley-VCH; 2009. p. 133–7.
[56] Köster W, Franz H. Met Rev 1961;6:1.
[57] Friák M, Šob M, Vitek V. Phys Rev B 2003;68:184101.
[58] Šob M, Friák M. Intermetallics 2009;17:523.
[59] Rutt HN, Nicola JH. J Phys C: Solid State Phys 1974;7:4522.
[60] Counts WA, Friák M, Raabe D, Neugebauer J. Acta Mater 2009;57:69.
[61] Ma Y, Aichmayer B, Paris O, Fratzl P, Meibom A, Metzler RA, et al. PNAS 2009;106:6048.